Supporting Information for

Laser Ablation Nanoarchitectonics of Au-Cu Alloys Deposited on TiO_2 Photocatalyst Films for Switchable Hydrogen Evolution from Formic Acid Dehydrogenation

Dachao Hong,[,‡] Aditya Sharma,[‡] Dianping Jiang,[†] Elena Stellino,[§] Tomohiro Ishiyama,[▽] Paolo Postorino,[O] Ernesto Placidi,[O] Yoshihiro Kon,[‡] and Kenji Koga,[*,†]*

[‡]Interdisciplinary Research Center for Catalytic Chemistry, [†]Nanomaterials Research Institute, [▽]Research Institute for Energy Conservation, National Institute of Advanced Industrial Science and Technology (AIST) 1-1-1 Higashi, Tsukuba, Ibaraki 305-8565, Japan

[§]Physics and Geology Department, University of Perugia, Via Alessandro Pascoli, 06123 Perugia, Italy

[O]Physics Department, Sapienza University of Rome, Piazzale Aldo Moro 5, 00185 Rome, Italy*

To whom correspondence should be addressed.

E-mail: hong-d@aist.go.jp (D.H.), k.koga@aist.go.jp (K.K.)

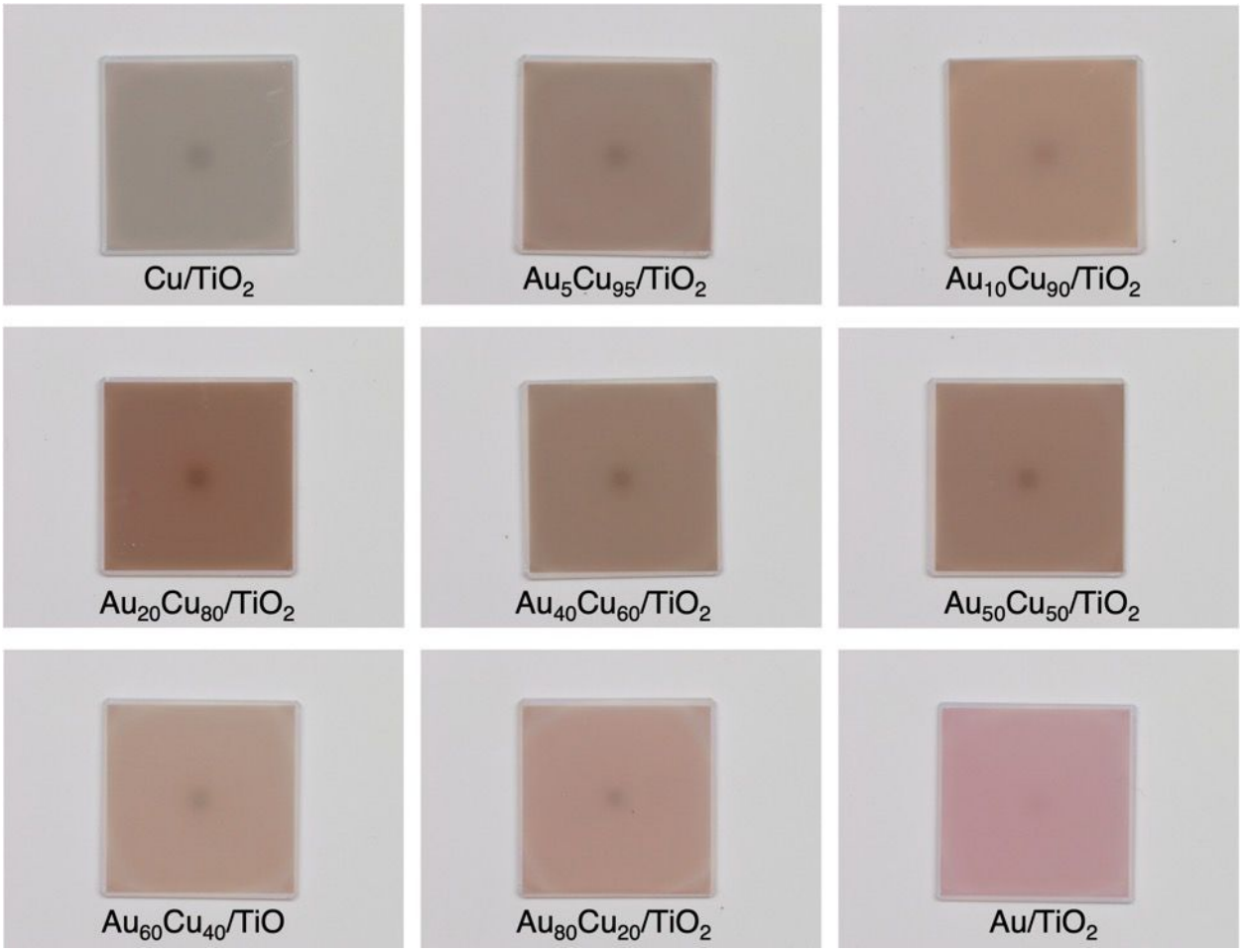

Figure S1. Images of the as prepared Au_xCu_{100-x}/TiO_2 particulate films with the size of 2.0 × 2.0 cm.

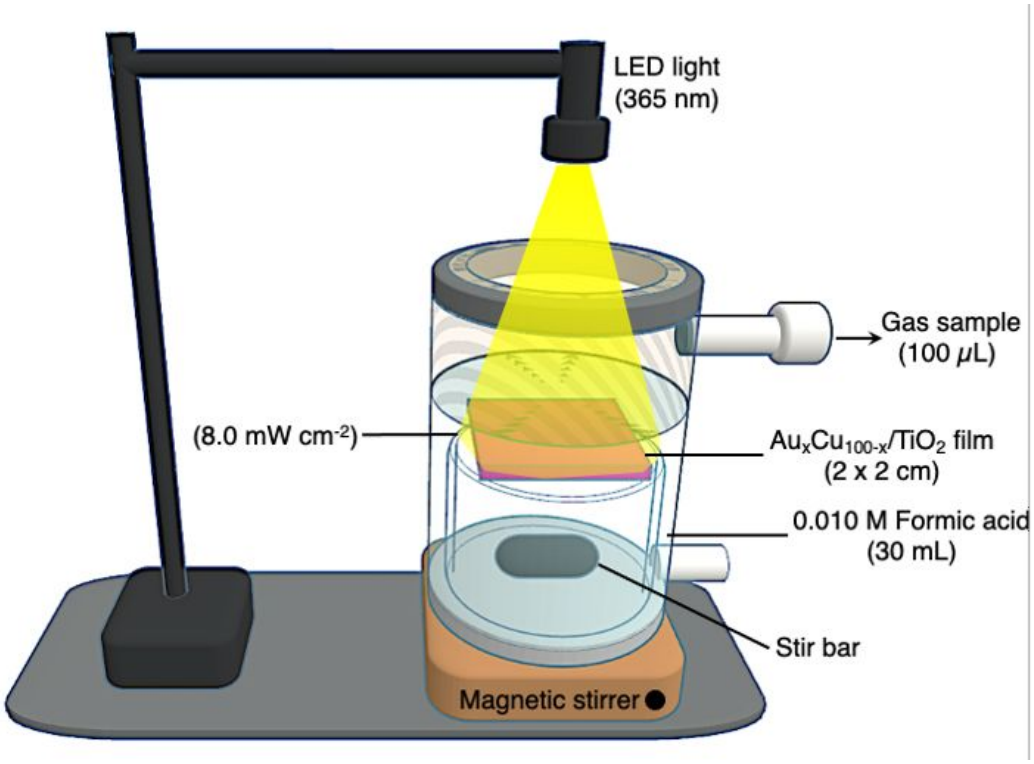

Figure S2. Experimental setup of photocatalytic system for H_2 production from formic acid dehydrogenation.

Table S1. Lattice parameters and Au contents of Au_xCu_{100-x} alloy NPs.

Photocatalysts	Lattice parameters[a] (nm)	Au ratio[b] (%)	Au amount[c] (nmol)	Au & Cu amount[c] (nmol)	Surface Au ratio[d] (%)
Cu/TiO_2	0.362	0	0	67	0
Au_5Cu_{95}/TiO_2	0.365	5.6	6.3	66	4.3
$Au_{10}Cu_{90}/TiO_2$	0.368	10.4	38	238	12.1
$Au_{20}Cu_{80}/TiO_2$	0.373	19.6	20	96	20.8
$Au_{40}Cu_{60}/TiO_2$	0.383	38.5	61	135	40.4
$Au_{50}Cu_{50}/TiO_2$	0.389	52.0	24	96	49.5
$Au_{60}Cu_{40}/TiO_2$	0.394	62.8	36	63	59.4
$Au_{80}Cu_{20}/TiO_2$	0.402	82.0	45	57	78.1
Au/TiO_2	0.409	100	36	36	100

[a] Calculated from XRD data. [b] Estimated from Vegard's law. [c] Determined by ICP-MS measurements. [d] Determined by XPS measurements.

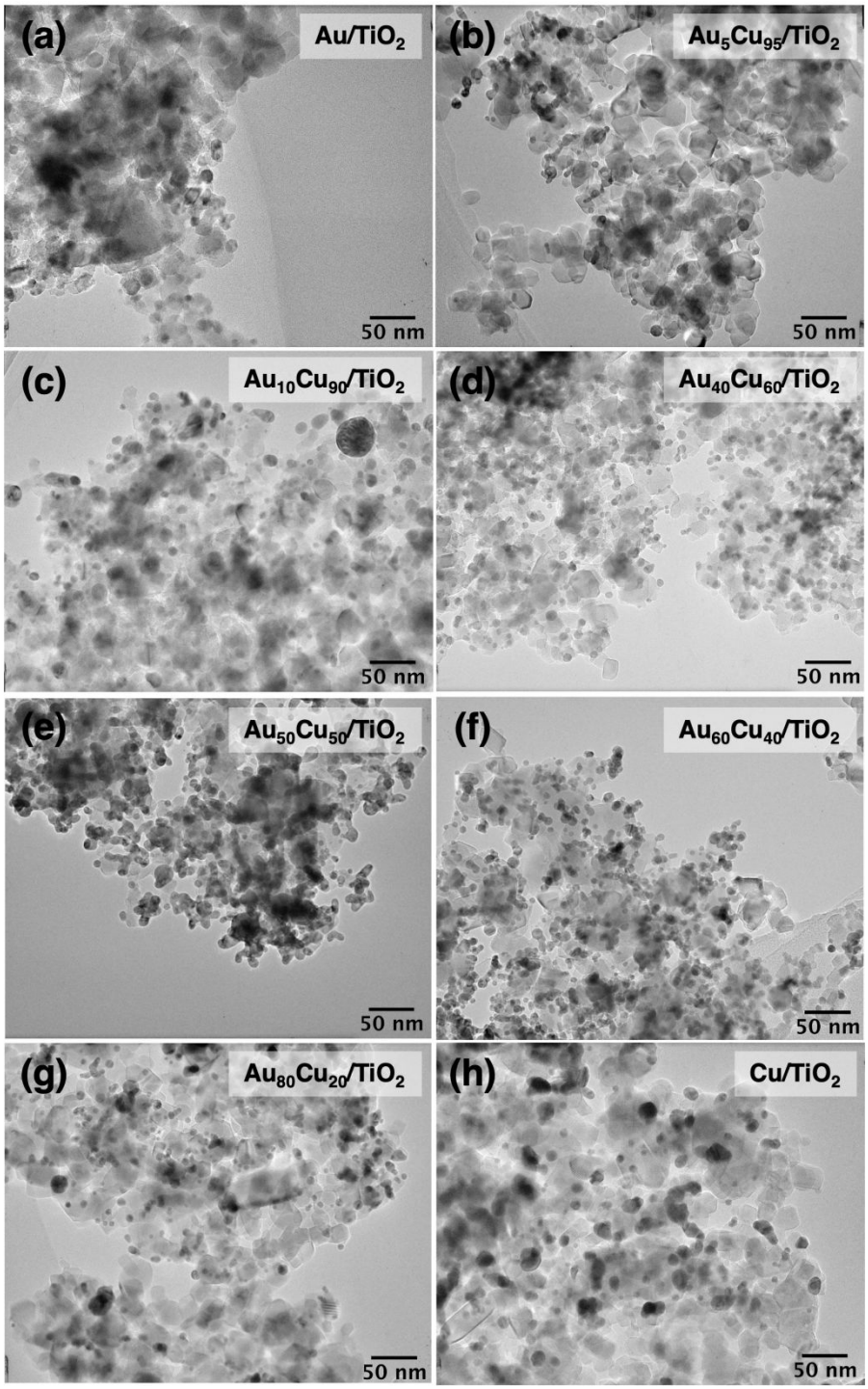

Figure S3. TEM images of (a) Au /TiO_2, (b) Au_5Cu_{95}/TiO_2, (c) $Au_{10}Cu_{90}/TiO_2$, (d) $Au_{40}Cu_{60}/TiO_2$, (e) $Au_{50}Cu_{50}/TiO_2$, (f) $Au_{60}Cu_{40}/TiO_2$, (g) $Au_{80}Cu_{20}/TiO_2$, and (h) Cu/TiO_2.

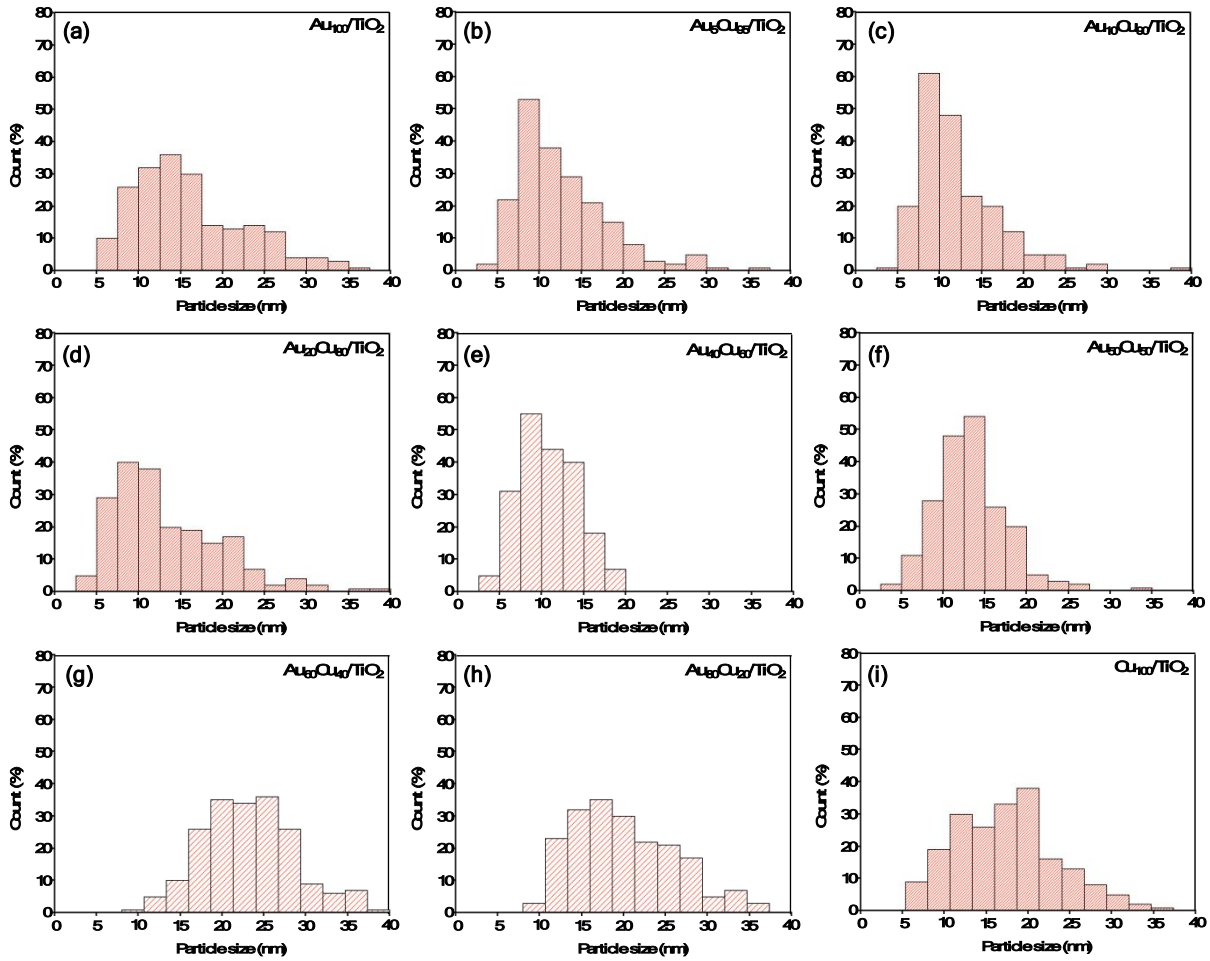

Figure S4. Particle size distribution of (a) Au (b) Au_5Cu_{95}, (c) $Au_{10}Cu_{90}$, (d) $Au_{20}Cu_{80}$, (e) $Au_{40}Cu_{60}$, (f) $Au_{50}Cu_{50}$, (g) $Au_{60}Cu_{40}$, (h) $Au_{80}Cu_{20}$ and (i) Cu deposited on TiO_2 films.

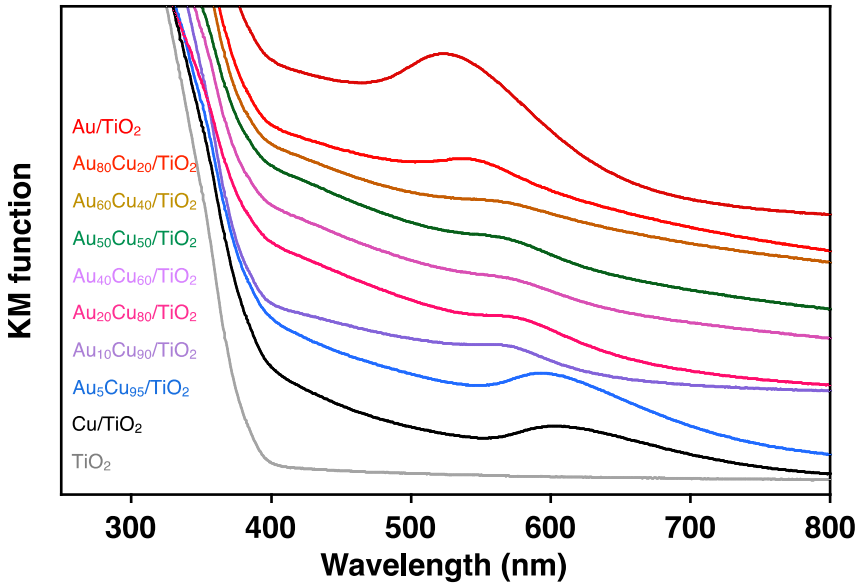

Figure S5. Diffuse reflectance UV-vis spectra of Au_xCu_{100-x}/TiO_2 (x = 0–100) and TiO_2 photocatalyst films.

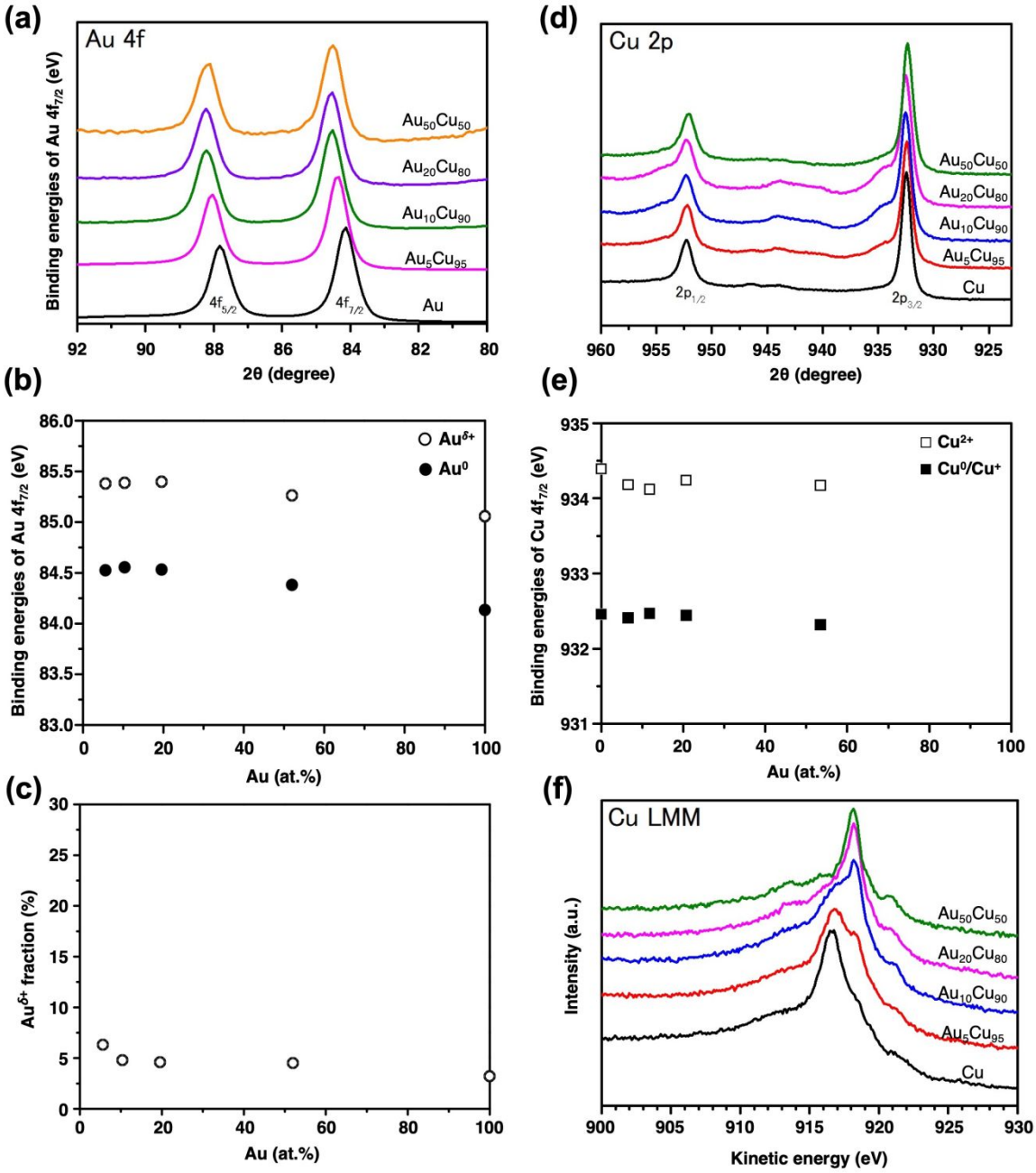

Figure S6. (a) XPS spectra of Au 4f, (b) the deconvoluted Au^0 and $Au^{\delta+}$ peaks values plotted against Au ratio (c) relative $Au^{\delta+}$ fraction plotted against Au ratio, (d) XPS spectra of Cu 2p, (e)

Cu $2p_{3/2}$ (Cu^{2+} and Cu^{0}/Cu^{+}) binding energy plotted against Au ratio and (f) Cu LMM spectra obtained from the Au–Cu/CP (carbon paper).

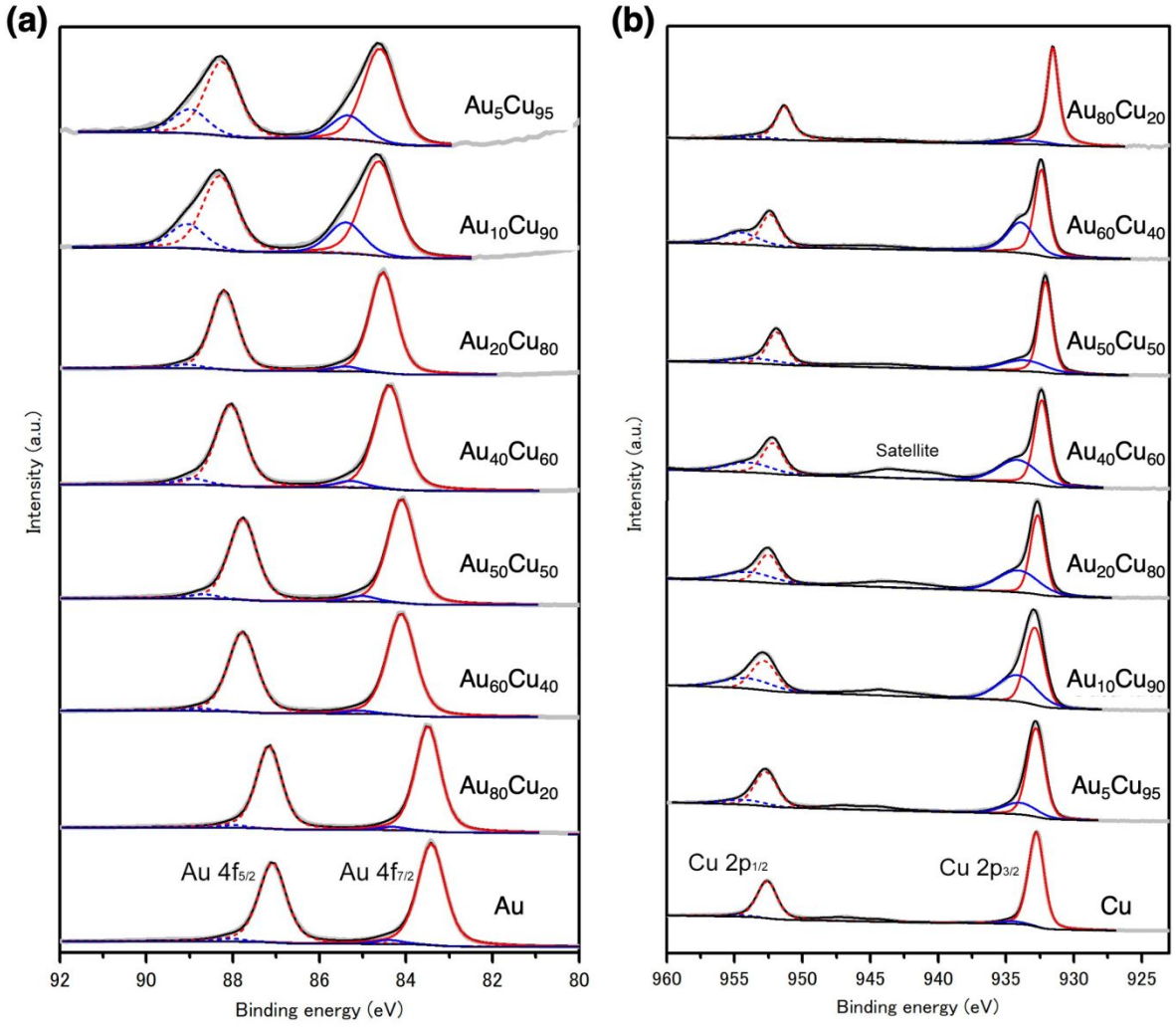

Figure S7. XPS spectra of (a) the deconvoluted Au 4f (b) Cu 2p peaks of different Au–Cu alloy NPs deposited on TiO_2 films.

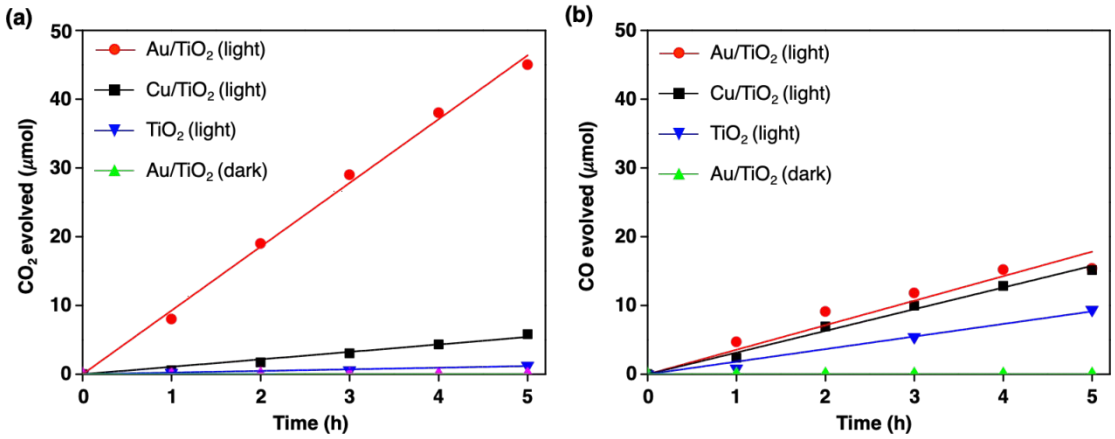

Figure S8. Time courses of (a) CO_2 and (b) CO evolution by irradiation (365 nm, 8.0 mW cm^{-2}) of TiO_2, Cu/TiO_2 and Au/TiO_2 and Au/TiO_2 photocatalysts under dark in formic acid solutions (0.010 M, 30 mL).

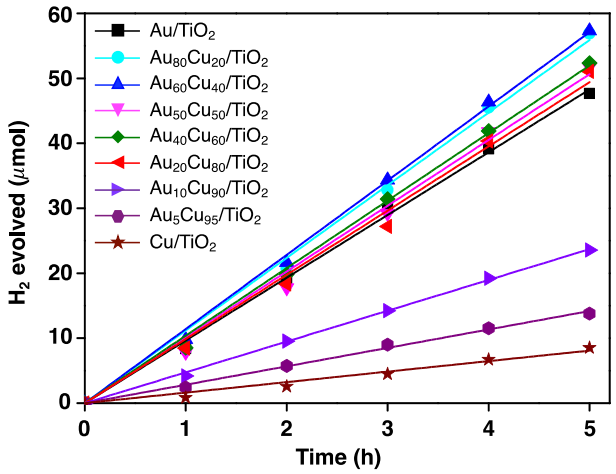

Figure S9. Time courses of H_2 evolution by the irradiation (365 nm, 8.0 mW cm^{-2}) of Au_xCu_{100-x}/TiO_2 (x = 0–100) photocatalysts in formic acid solutions (0.010 M, 30 mL).

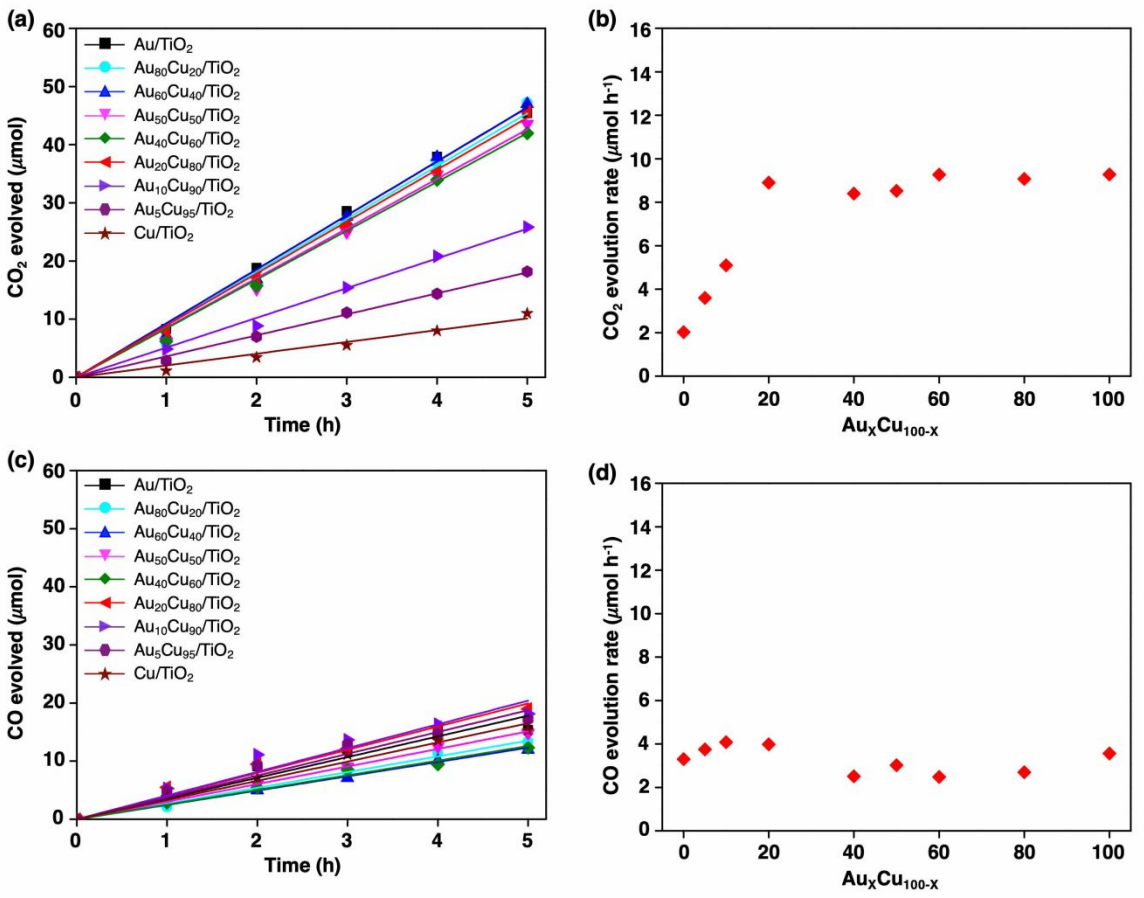

Figure S10. Time courses of (a) CO_2 and (c) CO evolution by irradiation (365 nm, 8.0 mW cm^{-2}) of Au_xCu_{100-x}/TiO_2 (x = 0–100) photocatalysts in formic acid solutions (0.010 M, 30 mL) and (b) CO_2 and (d) CO evolution rates plotted against the Au ratios.

Table S2. Comparison of photocatalytic H_2 evolution from formic acid dehydrogenation.

Photocatalyst	Light source	Light intensity (mW cm^{-2})	Weight, (mg)	Temp. (°C)	H_2 rate (μmol g^{-1} h^{-1})	Ref.
Au/TiO_2	LED (365 nm)	8	0.4	25	24200	This study
$Au_{20}Cu_{80}$ /TiO_2	LED (365 nm)	30	0.4	25	62500	This study
Au (1wt%) /$SrTiO_3$	Hg lamp	2.3	200	45	647	[R1]
Au-La_2O_3 /TiO_2	Xe lamp	99.5	100	50	1784	[R2]
Au/Pd NDBs-0.05	Visible-NIR (>420 nm)	100	-	15	1050	[R3]
Pd tipped Au NRs	Visible-NIR (>420 nm)	100	0.008	25	10500	[R4]
Pd dotted Ag@Au	Xe lamp (>400nm)	60	0.18	25	30000	[R5]
$MoS_2/Zn_3In_2S_6$	Xe lamp (>420nm)	-	0.1	4	7425	[R6]
Pt/g-C_3N_4	Simulated solar light	70	80	6	1590	[R7]
FHS/H-mag	Simulated solar light	-	15	25	470	[R8]
Pd-tipped Au NRs	Xe lamp	160	-	28	42800	[R9]
AgPd@Pd/TiO_2	Xe lamp	-	28.1	27	468000	[R10]
AgPd@Pd/TiO_2	Without light	-	28.1	27	294000	[R10]
Co-Ni/CdS NRs	Xe lamp (>420nm)	100	0.15	25	32600	[R11]
CdS/CoP@RGO	LED (>420nm)	11	1.0	25	182000	[R12]

References:

(R1) Puangpetch, T.; Chavadej, S.; Sreethawong, T. Hydrogen Production over Au-Loaded Mesoporous-Assembled $SrTiO_3$ Nanocrystal Photocatalyst: Effects of Molecular Structure and Chemical Properties of Hole Scavengers. *Energy Convers. Manag.* **2011**, 52 (5), 2256–2261.

(R2) Wu, M.; Zhang, M.; Lv, T.; Guo, M.; Li, J.; Okonkwo, C. A.; Liu, Q.; Jia, L. The Effect of Calcination Atmosphere upon the Photocatalytic Performance of Au-La2O3/TiO2 for Hydrogen Production from Formic Acid. *Appl. Catal. A Gen.* **2017**, 547, 96–104.

(R3) Yin, Y.; Yang, Y.; Zhang, L.; Li, Y.; Li, Z.; Lei, W.; Ma, Y.; Huang, Z. Facile Synthesis of Au/Pd Nano-Dogbones and Their Plasmon-Enhanced Visible-to-NIR Light Photocatalytic Performance. *RSC Adv.* **2017**, 7 (59), 36923–36928.

(R4) Zheng, Z.; Tachikawa, T.; Majima, T. Plasmon-Enhanced Formic Acid Dehydrogenation Using Anisotropic Pd-Au Nanorods Studied at the Single-Particle Level. *J. Am. Chem. Soc.* **2015**, 137 (2), 948–957.

(R5) Tong, F.; Lou, Z.; Liang, X.; Ma, F.; Chen, W.; Wang, Z.; Liu, Y.; Wang, P.; Cheng, H.; Dai, Y.; Zheng, Z.; Huang, B. Plasmon-Induced Dehydrogenation of Formic Acid on Pd-Dotted Ag@Au Hexagonal Nanoplates and Single-Particle Study. *Appl. Catal. B Environ.* **2020**, 277, 119226.

(R6) Zhang, S.; Duan, S.; Chen, G.; Meng, S.; Zheng, X.; Fan, Y.; Fu, X.; Chen, S. MoS2/Zn3In2S6 Composite Photocatalysts for Enhancement of Visible Light-Driven Hydrogen Production from Formic Acid. *Chinese J. Catal.* **2021**, 42 (1), 193–204.

(R7) Wang, J.; Wang, X.; Qiu, L.; Wang, H.; Duan, L.; Kang, Z.; Liu, J. Photocatalytic Selective H_2 Release from Formic Acid Enabled by CO_2 Captured Carbon Nitride. *Nanotechnology* **2021**, 32 (27), 275404.

(R8) El-Hosainy, H.; Tahawy, R.; Esmat, M.; El-Kemary, M.; Ide, Y. Immobilization of Iron Minerals on a Layered Silicate for Enhancing Its Solar Photocatalytic Activity toward H2 Production. Front. Energy Res. **2021**, 9, 83.

(R9) Gao, W.; Liu, Q.; Zhao, X.; Cui, C.; Zhang, S.; Zhou, W.; Wang, X.; Wang, S.; Liu, H.; Sang, Y. Electromagnetic Induction Effect Induced High-Efficiency Hot Charge Generation and Transfer in Pd-Tipped Au Nanorods to Boost Plasmon-Enhanced Formic Acid Dehydrogenation. *Nano Energy* **2021**, 80, 105543.

(R10) Tsuji, M.; Shimamoto, D.; Uto, K.; Hattori, M.; Ago, H. Enhancement of Catalytic

Activity of AgPd@Pd/TiO2 Nanoparticles under UV and Visible Photoirradiation. *J. Mater. Chem. A* **2016**, 4 (38), 14649–14656.

(R11) Nasir, J. A.; Hafeez, M.; Arshad, M.; Ali, N. Z.; Teixeira, I. F.; McPherson, I.; Zia-ur-Rehman; Khan, M. A. Photocatalytic Dehydrogenation of Formic Acid on CdS Nanorods through Ni and Co Redox Mediation under Mild Conditions. *ChemSusChem* **2018**, 11 (15), 2587–2592.

(R12) Cao, S.; Chen, Y.; Wang, H.; Chen, J.; Shi, X.; Li, H.; Cheng, P.; Liu, X.; Liu, M.; Piao, L. Ultrasmall CoP Nanoparticles as Efficient Cocatalysts for Photocatalytic Formic Acid Dehydrogenation. *Joule* **2018**, 2 (3), 549–557.

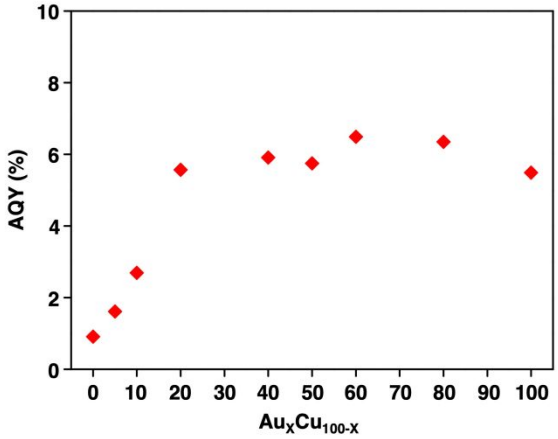

Figure S11. Apparent quantum yields obtained for Au_xCu_{100-x}/TiO_2 photocatalysts under LED irradiation (365 nm, 8.0 mW cm^{-2}) in formic acid solutions (0.010 M, 30 mL)

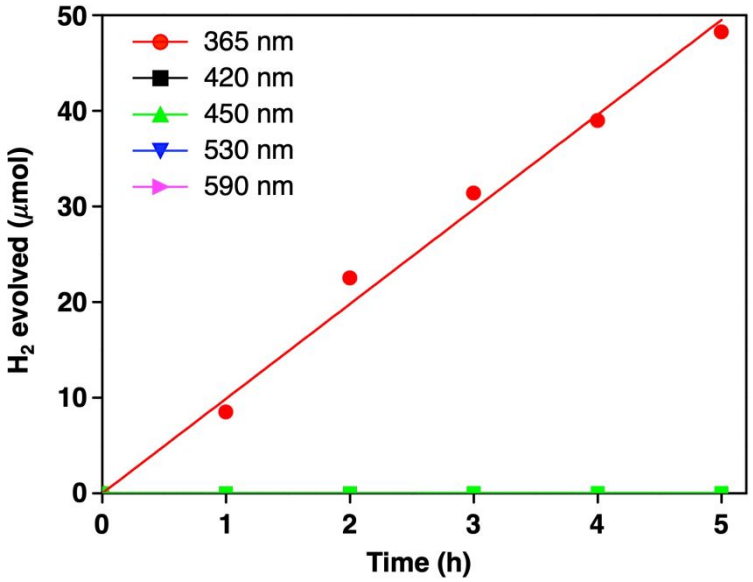

Figure S12. Time courses of H_2 evolution on $Au_{20}Cu_{80}/TiO_2$ by the irradiation of different wavelengths (λ = 365, 420, 450, 530 and 590 nm) in formic acid solutions (0.010 M, 30 mL).

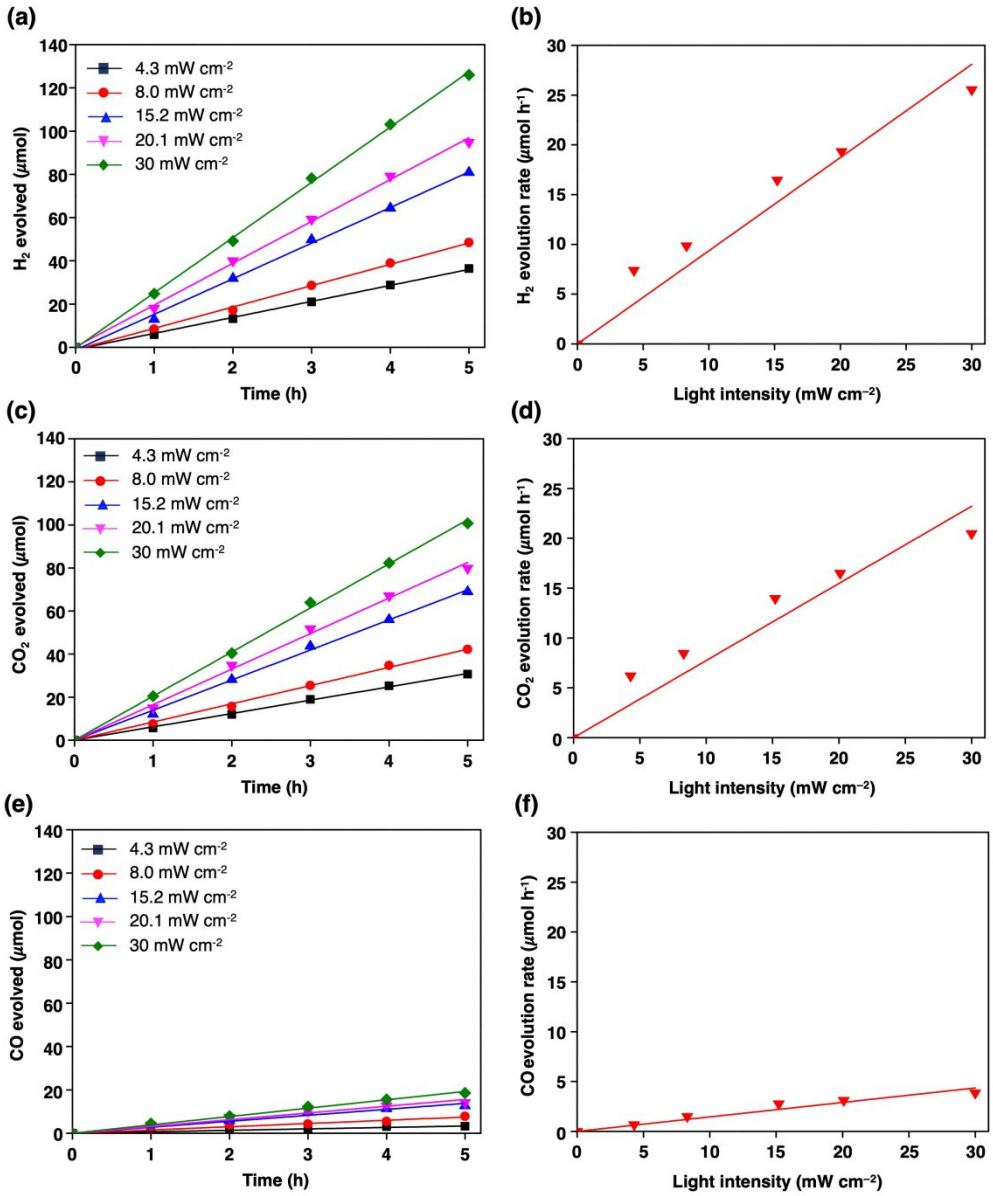

Figure S13. (a) The time courses of the H_2 evolution on $Au_{20}Cu_{80}/TiO_2$ by the irradiation of different light intensities (4.3–30 mW cm^{-2}) and (b) the dependence of the H_2 evolution on light intensity. (c) the time courses of CO_2 evolution and (d) the dependence of the CO_2 evolution rates on the light intensity. (e) the time courses of CO evolution and (f) the dependence of the CO evolution rates on the light intensity.

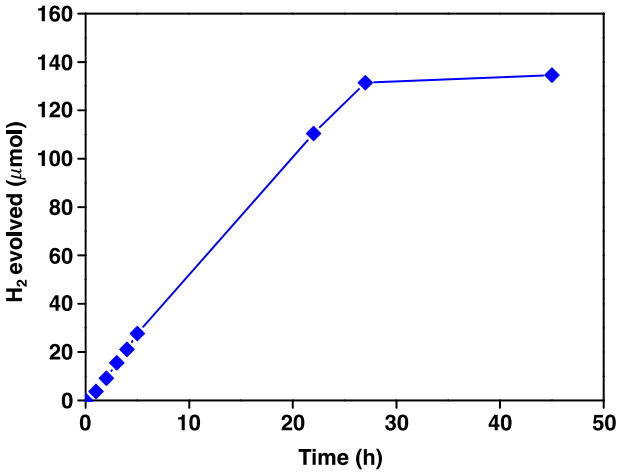

Figure S14. Long term duration of $Au_{20}Cu_{80}/TiO_2$ in the H_2 evolution from FA dehydrogenation under LED irradiation.

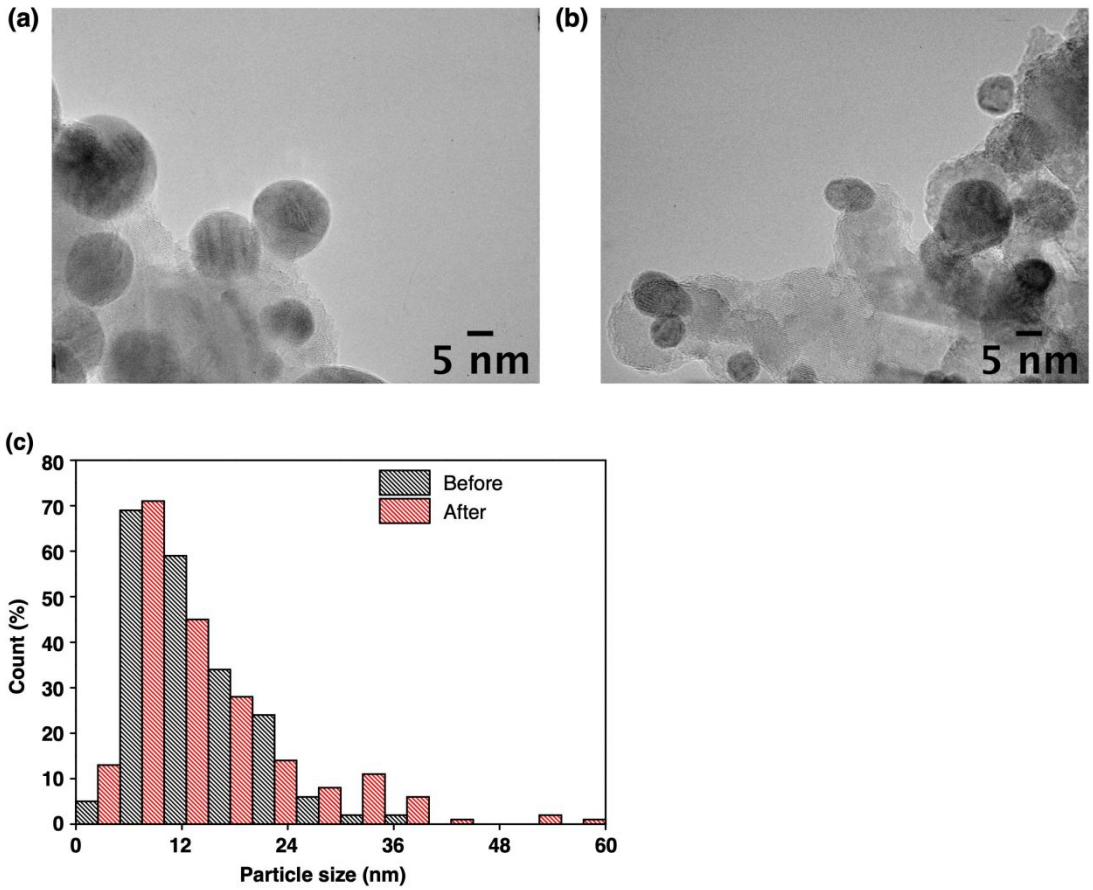

Figure S15. The HR-TEM images of $Au_{20}Cu_{80}/TiO_2$ photocatalyst films (a) before and (b) after reaction for the H_2 evolution from formic acid dehydrogenation. (c) Particle size distribution of $Au_{20}Cu_{80}/TiO_2$ photocatalyst film before and after the H_2 evolution from formic acid dehydrogenation.

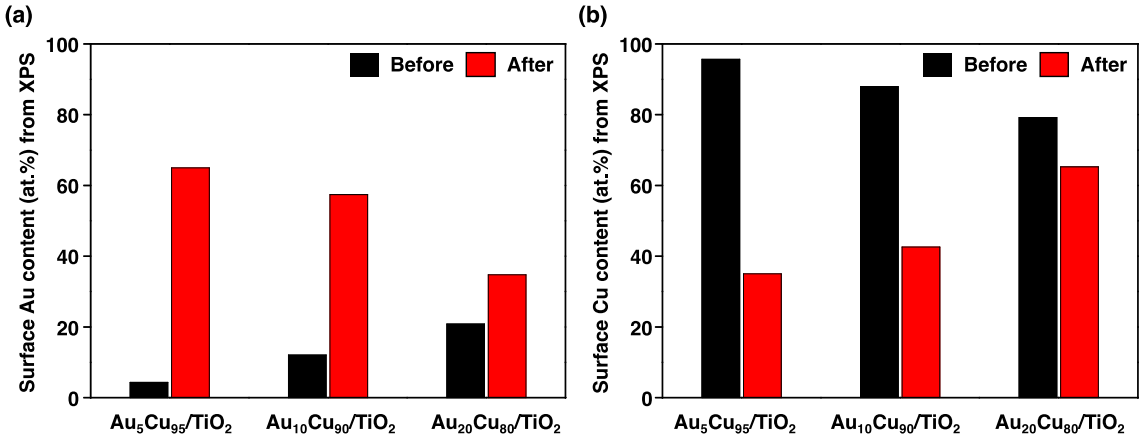

Figure S16. Surface Au (a) and Cu (b) contents of the Au-Cu/TiO_2 films estimated by XPS data analyses of the spectra before and after the reactions. Comment: The surface Cu contents were estimated by $Au4f_{7/2}$ and $Cu2p_{3/2}$ areas normalized with cross-section factors as the reported literature.[R13]

Reference:

(R13) Scofield, J. H., Hartree-Slater subshell photoionization cross-sections at 1254 and 1487 eV. *J. Electron Spectros. Relat. Phenomena* **1976**, (8) 129–137.

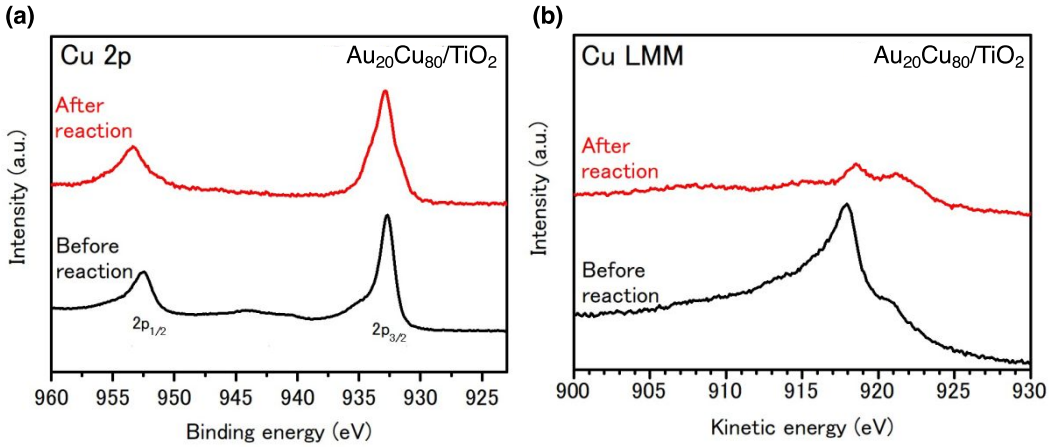

Figure S17. (a) The XPS spectra of Cu 2p and (b) Cu LMM analysis before and after the H_2 evolution from formic acid dehydrogenation.

Table S3. Ohmic resistance of Au_xCu_{100-x}/TiO_2 photocatalysts in formic acid solution analyzed with an equivalent circuit model.

Sample	R_{sol} /Ω	R_{et} / Ω	R_{re} / Ω
Au	285	476	184
$Au_{50}Cu_{50}$	267	828	345
$Au_{20}Cu_{80}$	266	957	513
$Au_{10}Cu_{90}$	304	1020	1051
Au_5Cu_{95}	294	1267	628
Cu	295	793	679

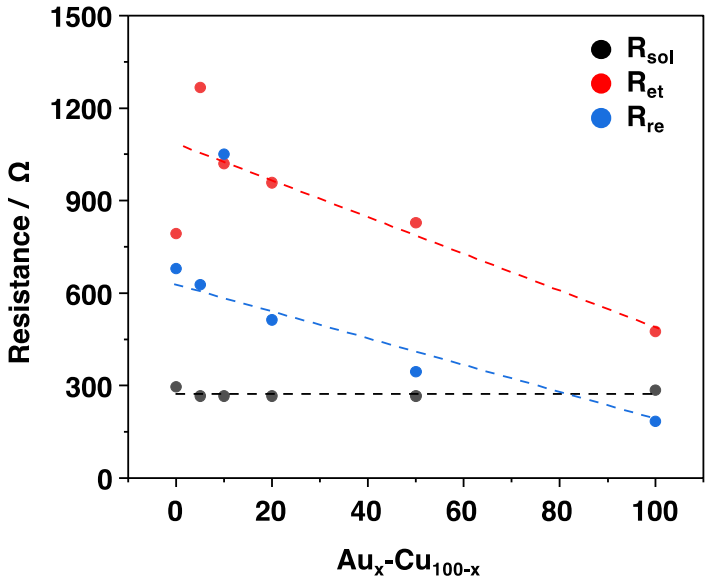

Figure S18. Plots of R_{sol}, R_{et} and R_{re} against Au content of Au-Cu/TiO_2 obtained from the EIS measurements under LED irradiation in formic acid (0.010 M).